Macromolecules

pubs.acs.org/Macromolecules Article

High-Strength and Excellent Self-Healing Polyurethane Elastomer Based on Rigid Chain Segment Reinforcement

Li-Quan Huang,[‖] Hua-Xin Huang,[‖] Ning Yu, Chang-Zhou Chen, Yang Liu, Guo-Hua Hu, Jun Du, and Hui Zhao*

Cite This: *Macromolecules* 2025, 58, 1425−1434 Read Online

ACCESS | Metrics & More | Article Recommendations | Supporting Information

ABSTRACT: Owing to their extensive application scope, elastomers that combine high strength and excellent self-healing efficiency have always attracted significant attention and are still a contradiction. In this study, a novel PU elastomer was prepared by combining rigid poly(amic acid) (PAA) chain segments and 3,3-dithiodipropionic dihydrazide (DPH) containing sextuple hydrogen-bonding units and disulfide bonds. The prepared elastomer exhibited a high tensile strength of 50.1 MPa and a high toughness of 144.2 MJ/m^3. The rigid PAA chain segments serve as a rigid framework, significantly enhancing the mechanical strength of the elastomer. Meanwhile, DPH with sextuple hydrogen-bonding units and disulfide bonds enabled the elastomer to exhibit an excellent self-healing efficiency of 96.1% after 12 h at 80 °C. Additionally, the strong and reversible cross-linking of the hydrogen-bonding arrays in the elastomer endows it with excellent mechanical strength, self-healing ability, and recyclability, allowing it to be recycled after hot pressing and dissolution.

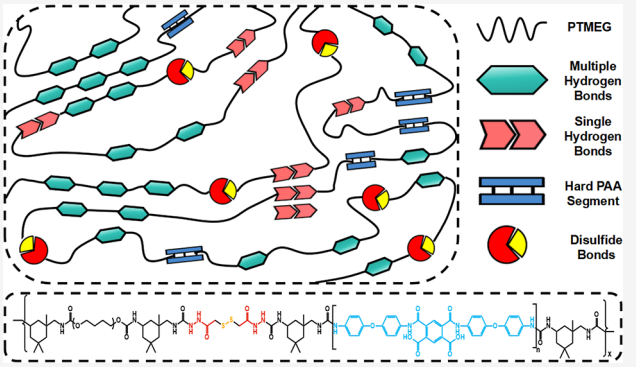

1. INTRODUCTION

Polyurethane (PU) elastomers have a wide range of applications in the human daily life, such as in automotive,[1−3] electronics,[4−9] and medical fields,[10−13] due to their excellent flexibility and resilience. For the sustainable development of the economy, researchers are now committed to endowing elastomer materials with self-healing performance and recycling performance,[14] to reduce their maintenance costs, extend their service life, and reduce the consumption of raw materials. The depletion and difficult recycling of elastomer materials in the use process have caused a serious waste of resources and environmental pollution.[15,16] Therefore, the development of PU elastomer materials with high mechanical strength, self-healing, and recyclability is of great significance to build a sustainable society.

However, the simultaneous realization of high strength and high self-healing efficiency of PU elastomers is contradictory.[17,18] In terms of microstructure property relationships, the high strength of PU elastomers is dependent on the specific structure and form of action of the molecular chains.[19] Highly regularized molecular chains promote close packing.[20] This limits chain movement and enhances intermolecular interactions,[21] thereby increasing tensile strength. High self-healing efficiency requires PU elastomers to introduce dynamic covalent bonds;[22] the reversibility of such bonds enables PU chain rearrangements and interactions to achieve self-healing when the material suffers damage.[23] Traditional high-strength elastomers need to build a solid cross-linked structure to strengthen the mechanical properties, but the cross-linked network is difficult to destroy and reconstruct, making the material unable to be healed and recycled effectively. Although dynamic cross-linking in self-healing elastomers presents the advantage of self-healing, it struggles to fulfill the requirements of high-strength applications owing to the high mobility of molecular chains and the absence of a robust cross-linking structure. Therefore, the preparation of PU elastomer materials with both high mechanical strength and efficient self-healing performance is still a great challenge.[24]

To effectively enhance the strength of polymer materials, researchers have been concentrating on approaches to reinforce cross-linked elastomers. There are two commonly adopted enhancement methods: (1) doping nanofillers, such as carbon nanotubes,[25] nanosilica,[26] and MXene,[27,28] to improve strength. Nevertheless, when using nanofiller modification, dispersion of the nanofiller becomes a critical issue. Nanofillers typically possess a high specific surface area, which often leads to their aggregation within the substrate. As a result, the

Received: January 2, 2025
Revised: January 17, 2025
Accepted: January 20, 2025
Published: January 24, 2025

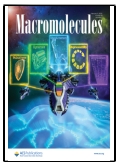

https://doi.org/10.1021/acs.macromol.5c00013
Macromolecules 2025, 58, 1425−1434

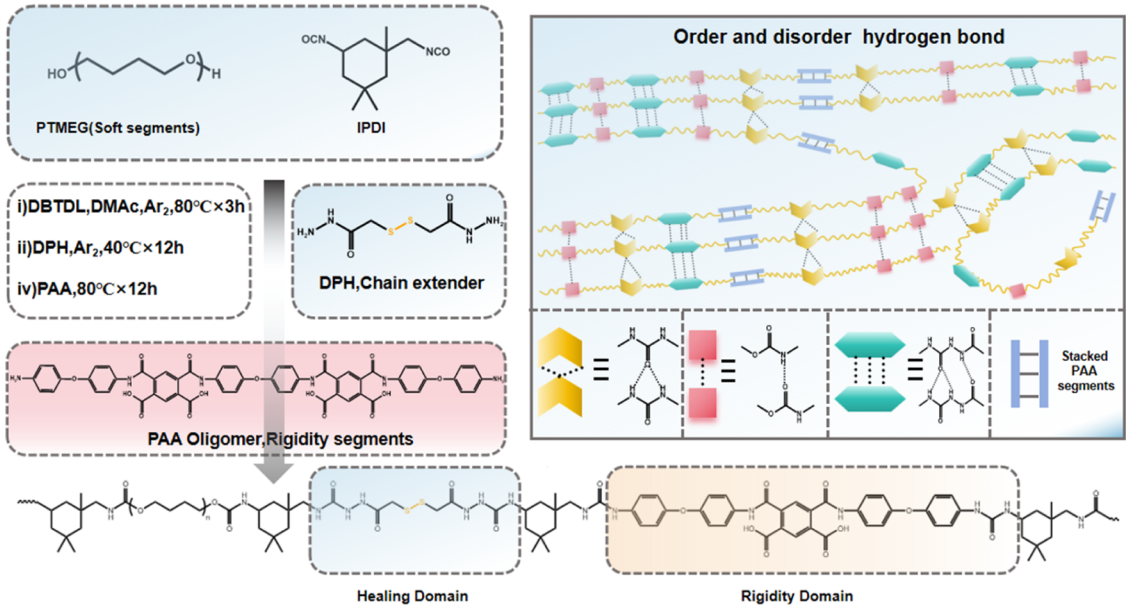

Figure 1. Synthesis process and molecular structure of PU elastomers.

interaction force and compatibility between the filler and the substrate decrease, ultimately giving rise to microphase separation. (2) Introducing sacrificial bonds (including hydrogen bonds,[29] coordination bonds,[30] etc.) and leveraging its dissociation and reorganization to dissipate energy.[31,32] Essentially, this involves designing the microphase separation[33] structure to strike a balance between mechanical strength and self-healing efficiency. Compared with the doping of nanofillers, the introduction of sacrificial bonds can effectively enhance the mechanical strength of elastomers, yet there is still room for further improvement. It is evident that both traditional enhancement methods have certain limitations and struggle to fully overcome the problem of balancing high mechanical strength with efficient self-healing performance. Recently, people are trying to utilize rigid chain segments[34] and incorporate hydrogen-bonding units and dynamic bonds in a chain extender;[35−37] the technical issue regarding the inability to balance high mechanical strength and efficient self-healing performance can be addressed.[38]

In this work, a self-healing PU elastomer with excellent mechanical properties was developed through an innovative approach. Specifically, rigid poly(amic acid) (PAA) chain segments are copolymerized into PU chain segments, functioning as fragments for enhancing mechanical strength. Meanwhile, a chain extender integrating sextuple hydrogen-bonding units and dynamic disulfide bonds is prepared. The introduction of the rigid chain segment, PAA, has significantly improved the mechanical properties of the PU elastomer. This rigid chain segment can increase the intermolecular interaction force, which renders the material more stable under the application of force and more effective in resisting deformation. As a result, the elastomer can achieve a tensile strength of up to 50.1 MPa. The synthesized 3,3-dithiobis(propionohydrazide) (DPH), which combines sextuple hydrogen-bonding units and disulfide bonds, endows the PU elastomer with excellent self-healing properties. Under heating conditions, it can reach a self-healing efficiency of 96.1%. The high-density hydrogen-bonding network formed by sextuple hydrogen-bonding units provides robust intermolecular bonding forces, facilitating rapid molecular rearrangement and rebinding when the material is damaged. Moreover, the dynamic disulfide bonds can be reorganized when materials are broken, enabling the damaged area of the material to achieve rigid self-healing. This innovative design not only offers new insights for enhancing the performance of PU elastomers but also serves as a valuable reference for the research and development of other polymer materials.

2. EXPERIMENTAL SECTION

2.1. Materials and Reagents. Poly(tetramethylene glycol) (PTMEG, M_n = 2000), isophorone diisocyanate (IPDI), and methanol (analytically pure) were supplied by Shanghai Macklin Biochemical Co., Ltd. Hydrazine hydrate (80%) and acetone (analytically pure) were purchased from Sinopharm Group. 4,4-Diaminodiphenyl ether (ODA) and pyromellitic dianhydride (PMDA) were provided by Tianjin Zhong Tai Science and Technology Materials Co., Ltd. *N*,*N*-Dimethylacetamide (DMAc) was provided by Energy Chemical. Before the experiment, PTMEG should be dried under vacuum at 110 °C for 2 h.

2.2. Synthesis of DPH. 3,3′-Dithiopropionic acid dimethylester (1.19 g, 4.2 mmol) was dissolved in dry methanol (25 mL). Subsequently, hydrazine hydrate (1.24 mL, 25 mmol) was added, and the reaction mixture was stirred overnight under room temperature conditions. The resulting suspension was then filtered, and the obtained white solid was washed successfully with methanol (10 mL), water (2 mL), and methanol (5 mL). Finally, a DPH white solid was acquired. The structure of DPH was confirmed by ^{1}H NMR spectroscopy (Figure S1, Supporting Information) ^{1}H NMR (600 MHz, DMSO-d_6, ppm): 9.05 (s, 2H, *N*−NH−C(O)), 4.21 (s, 4H, NH_2−N−C(O)), 2.88 (t, 4H, C(O)−C−CH_2−S), 2.40 (t, 4H, N−C(O)−CH_2−C).

2.3. Synthesis of PAA. The molar ratio of PMDA:ODA is 1:2; the synthesis process is as follows: under an atmosphere of nitrogen, ODA (1.12 g, 40 mmol) was added into a 100 mL three-necked flask, and 80 mL of DMAc was added with full stirring; after complete dissolution, PMDA (2.22 g, 320 mmol) was weighed into the three-necked flask, and the reaction solution was stirred in an ice-water bath for 12 h. A light-green solution was obtained and poured into excess ethanol to precipitate. The reaction solution was stirred in an ice-water bath for 12 h to obtain a light-green poly(amic acid) solution. The poly(amic acid) solution was poured into an excess of ethanol for precipitation, and the suspension was filtered to obtain a filter cake,

https://doi.org/10.1021/acs.macromol.5c00013
Macromolecules 2025, 58, 1425−1434

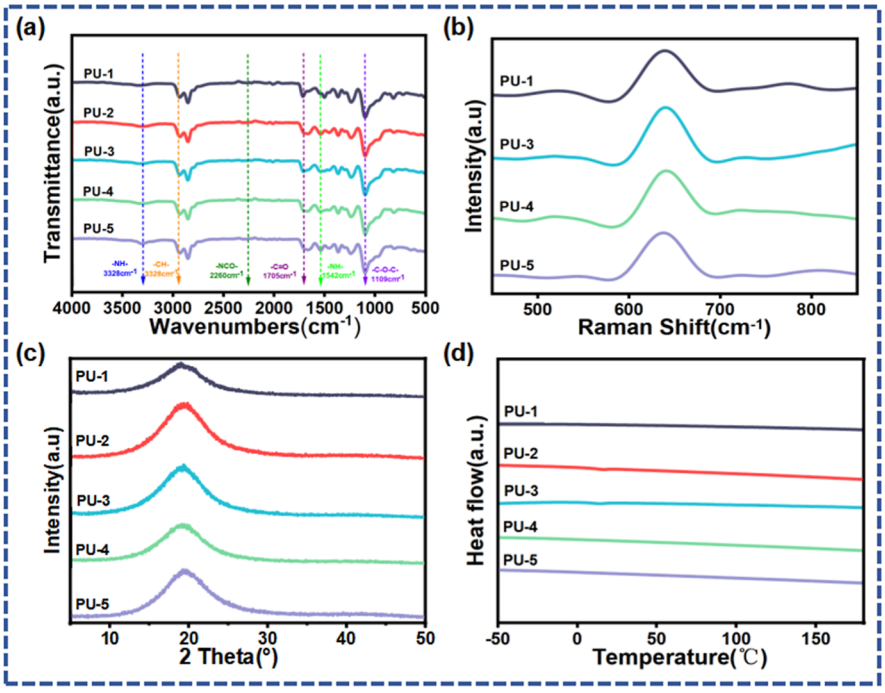

Figure 2. (a) FTIR of all PU samples; (b) Raman spectroscopic curves; (c) XRD of all PU samples; (d) DSC curves of all PU samples.

and the filter cake was washed with acetone three times and then placed in a 50 °C vacuum oven to dry for 48 h, to obtain a light-green amino-capped PAA ($H_2N-PAA-NH_2$) powder. The structure of $H_2N-PAA-NH_2$ was confirmed by ^1H NMR spectroscopy (Figure S2, Supporting Information), and the molecular weights result of H2N-PAA-NH2 was confirmed by gel permeation chromatography (Table S3 and Figure S10, Supporting Information).

2.4. Synthesis of the PU Elastomers. As an example, the synthesis of PU-3 was carried out as follows. First, PTMEG was added to a 250 mL dry three-necked flask and heated under vacuum at 115 °C for 0.5 h to remove the water. Next, a DMAc solution of IPDI and DBTDL was added into the reaction system under an argon atmosphere. Subsequently, the mixture was stirred continuously at 80 °C for 3 h, thus obtaining the IPDI-PTMEG prepolymer. After that, when the mixture was cooled to 40 °C, DPH was dissolved in DMAc. Then, the DPH solution was continuously added to the prepolymer solution under an argon atmosphere, and the stirring continued at 40 °C for 12 h. Subsequently, the system was warmed to 80 °C, and then the DMAc solution of amino-capped PAA was added to the mixture. The stirring was continued for 12 h to obtain the DMAc solution of the target PU elastomers. The feed masses of PTMEG, IPDI, PAA, and DPH were as follows: PTMEG (10 g), IPDI (2.23 g), PAA (0.485 g), and DPH (0.6 g). The synthesis process of the raw material is shown in Figure S3 and Table S1.

2.5. Synthesis of the PU-Control Elastomer. The synthesis of PU-control-1 was carried out as follows. First, PTMEG was added into a 250 mL dry three-necked flask and heated under vacuum at 115 °C for 0.5 h to remove the water. Then, a DMAc solution of IPDI and DBTDL was added to the reaction system. Subsequently, the mixture was stirred continuously at 80 °C for 3 h to obtain the IPDI-PTMEG prepolymer. After that, the DMAc solution of amino-capped PAA ($H_2N-PAA-NH_2$) was added and the mixture was stirred continuously at 80 °C for 12 h to obtain the DMAc solution of the control PU elastomer PU-control-1, and synthesis steps of PU-control-2 are also similar. The synthesis process of the raw material is shown in Figure S4 and Table S2.

3. RESULTS AND DISCUSSION

Figure 1 illustrates the molecular structure and interactions of high-strength and self-healing elastomers, which adopt a design strategy based on rigid oligomer chain segments to enhance mechanical properties. In the synthesis of PU, PTMEG was selected as the soft segment. It is abundant in ether bonds (−O−), and these ether bonds possess high flexibility, endowing the PU soft segment with excellent flexibility and elasticity. IPDI was chosen as the isocyanate for the hard segment. With its ring-like rigid structure and high steric hindrance, it facilitates the formation of an amorphous structure within the elastomer. DPH, containing dynamic disulfide bonds, was opted for as the chain extender. The synthetic route and NMR hydrogen spectra of DPH are presented in Figure S1 in the Supporting Information. DPH encompasses both dynamic bonds, and the multiple acylsemicarbazide group generated by the reaction between its terminal amino group and IPDI is more inclined to form a richer hydrogen bonds donor. Furthermore, its rigid structure also contributes to the enhancement of the mechanical properties. The synthetic route and NMR hydrogen spectrum of the relevant part are depicted in Figure S2 in the Supporting Information. A three-dimensional network of dynamically cross-linked linear polymers was designed and synthesized through stepwise copolymerization. Eventually, a series of target elastomers were obtained and named PU-1, PU-2, PU-3, PU-4, and PU-5; Figures S3 and S4 detail the specific synthesis steps, and Table S6 details the specific synthesis formula of PU elastomers.

Fourier transform infrared (FTIR) spectroscopy, Raman spectroscopy, and X-ray diffraction (XRD) tests were performed on the elastomers. The aim was to investigate the chemical structure and crystalline behavior of the polymers and to demonstrate the successful preparation of the target polymers. As shown in Figure 2a, there were no vibrational peaks at 2240−2280 cm^{-1} in the PU system. This verified the complete reaction of the −NCO group, indicating that all the IPDI monomers reacted completely and successfully to prepare the PU.[39] The characteristic peaks appearing at 3328 cm^{-1} and 1542 cm^{-1} are the stretching and bending vibration

https://doi.org/10.1021/acs.macromol.5c00013
Macromolecules 2025, 58, 1425−1434

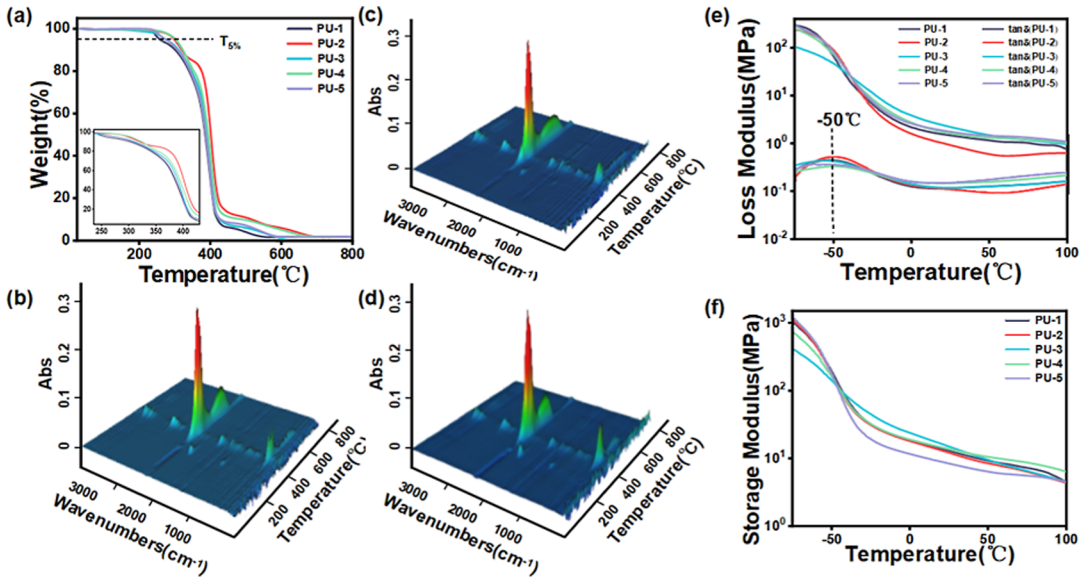

Figure 3. (a) TGA curves of PU samples; (b) TGA-IR spectroscopic images of PU-3; (c) TGA-IR spectroscopic images of PU-4; (d) TGA-IR spectroscopic images of PU-5; (e) loss modulus and tan δ of PU samples; (f) storage modulus of PU samples.

peaks of N−H in the urethane (−NH−COO−) group, respectively, and the appearance of the peak at 1705 cm^{-1} is attributed to the C═O bond in the urethane (−NH−COO−) group. Moreover, the vibrational broad peak at 1109 cm^{-1} is mainly attributed to the stretching vibration of C−O−C in the polyether molecular chain. The Raman spectra of the four samples are shown in Figure 2b, and it can be seen that raised C−S peaks are at 630 cm^{-1}.[40] This indicates that the disulfide bonds are successfully bonded into the PU chain. To gain a deeper understanding of the relationship between the structure and properties of the synthesized elastomers, microstructural characterization was carried out on all of the samples. As shown in the XRD spectra of Figure 2c, there is a broad amorphous diffraction peak at around 19.5° for all the samples. This suggests that all of the urethane elastomers exhibit an amorphous structure and that all of the samples are in an amorphous state at room temperature. Furthermore, to further confirm this amorphous characteristic from another perspective, differential scanning calorimetry (DSC) tests were carried out on all the samples as shown in Figure 2d. No heat absorption peaks were observed in the DSC curves, indicating that the PU is not able to crystallize in the temperature range from −80 to 190 °C. The presence of the amorphous structure indicates that the chain segments have enough space for chain movement, which facilitates dynamic reorganization. These results provide abundant and effective proof for the successful synthesis of PU.

To gain a more comprehensive understanding of the physical and chemical changes that the samples undergo during heat exposure, thermogravimetric/FTIR spectroscopy (TGA-IR) was employed to investigate the impact of PAA chain segments on the structure and thermal stability of PU elastomer. The TGA and TGA-IR spectra of all samples are presented in Figure 3. As can be seen from the TGA images in Figure 3a and DTG images in Figure S8, there are four distinct signal intervals, namely, 255−300 °C, 300−370 °C, 370−470 °C, and 470−800 °C. The initial decomposition temperatures ($T_{5\%}$) of the PU containing different mass ratios of PAA vary, yet none of them are lower than 255 °C. The temperature ranges of 255−300 °C represent the first stage of thermal decomposition, mainly corresponding to the dehydration stage of carboxy imination in PAA on PU. Notably, the weight loss rate slows down significantly with an increase in the PAA content. This might be attributed to the stable conjugated structure of the benzene ring, the enhanced intermolecular forces, and the hindrance to heat transfer and energy diffusion. The second stage, from 300 to 370 °C, is a subpeak of weight loss, primarily involving the decomposition of the polyether in the soft segment and urethane carbamate in the hard segment of PU. The third stage, ranging from 370 to 470 °C, mainly pertains to the decomposition of rigid groups such as aliphatic and aromatic rings in PU. It can be observed that during the second and third stages of heat loss, as the PAA content increases, the heat loss rate of the polymer decreases, and the temperature range of heat loss broadens. This is since the PAA in the PU exhibits higher heat resistance compared to the urethane. In this third stage of heat loss, an inflection point of the heat loss rate of PU elastomer occurs near 440 °C, which is mainly attributed to the decomposition of rigid groups like benzene rings. Moreover, an increase in the content of rigid groups within the polymer leads to the expansion of the thermal decomposition region in this stage. Overall, the above results suggest that the synthesized PU possesses good heat resistance, the thermogravimetric results of PU-control-1 and PU-control-2 also indicate that they exhibit excellent thermal stability (Figures S6 and S7, Supporting Information). Meanwhile, from the TGA-IR spectral images in Figure 3b−d, take PU-3 as an example; the decomposition products in the initial two degradation stages include C−CH_3 (at 1330 cm^{-1}), carbon monoxide (CO, within the range of 2040−2100 cm^{-1}), and carbon dioxide (CO_2, within the range of 2300−2400 cm^{-1}). The third stage (370−470 °C) of PU-4 and PU-5 is like that of PU-3 described above. In the third stage, the CO characteristic peak disappears, the CO_2 release reaches its maximum, a bending vibration peak appears at 669 cm^{-1}, and a hydroxyl characteristic band emerges within the range of 3600−3800 cm^{-1}. This stage corresponds to the decomposition of the thermally stable soft-segmented polyether. The thermal decomposition occurring at 470−800 °C can likely be

https://doi.org/10.1021/acs.macromol.5c00013
Macromolecules 2025, 58, 1425−1434

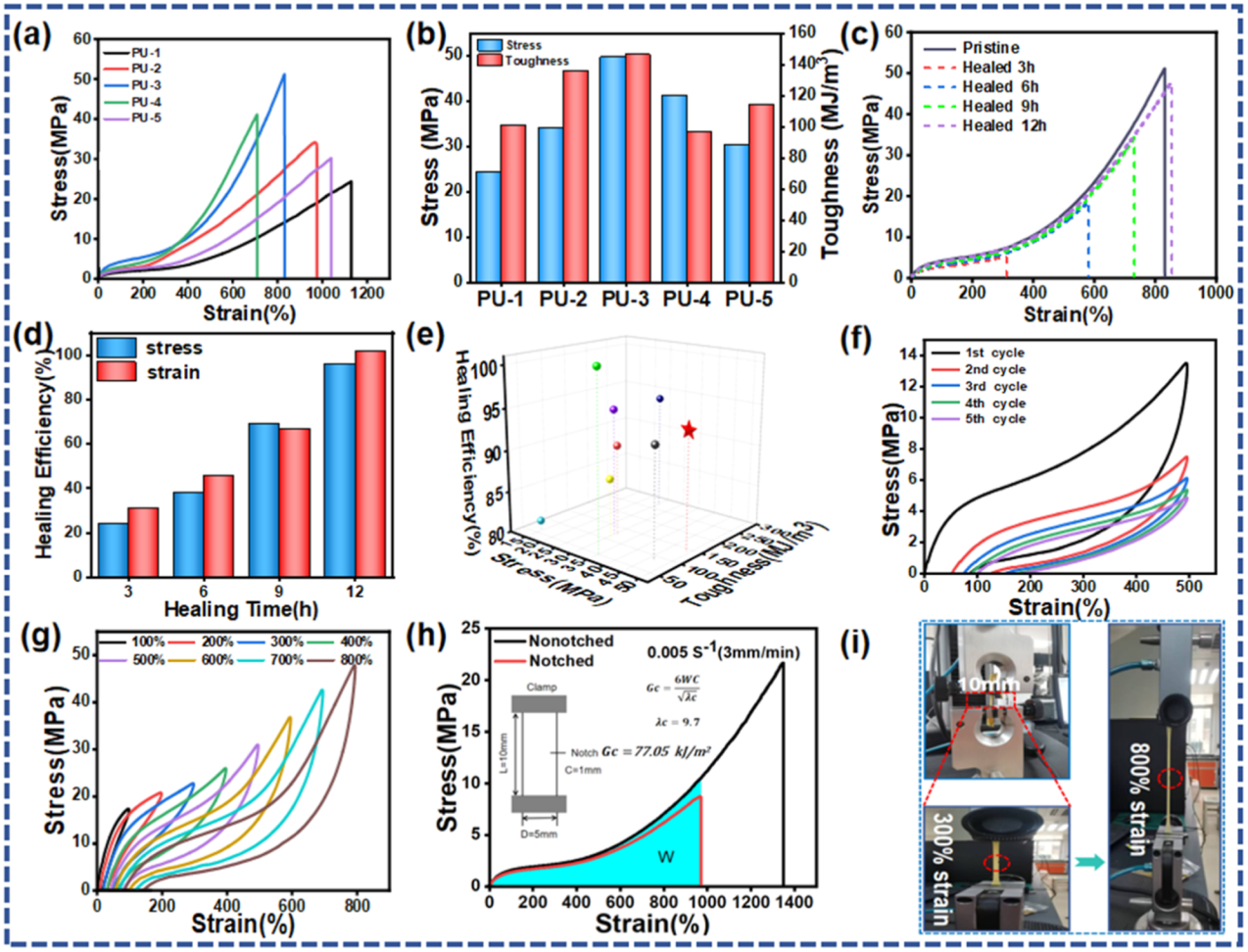

Figure 4. Mechanical properties of PU elastomer sample; (a) stress−strain curves; (b) toughness bar chart of different samples; (c) self-healing stress−strain curves of different samples; (d) self-healing efficiency bar chart of all samples; (e) performance comparison 3D diagram; (f) cyclic 5 times tensile test of PU-3 elastomer at a strain of 500%; (g) load−unload cycle curves of PU-3 with the strain increasing from 100% to 800%; (h) fracture energy; (i) photographs of notched PU-3 samples tensile up to 1360% strain;.

attributed to the complete decomposition of the polymer carbon skeleton.[41,42]

To investigate the dynamic viscoelastic properties of the fabricated PU, the temperature dependence of storage modulus, loss modulus, and tan δ was determined by the dynamic mechanical analyzer, and the temperature dependence curves of storage modulus (E′), loss modulus (E″), and tan δ of PU are shown in Figure 3e,f. The modulus properties of the PU elastomer material undergo continuous changes when the temperature gradually increased from −80 to 100 °C. At the initial stage of temperature increase, the multiple hydrogen bonds, although subject to certain thermal effects, still dominate the interactions between molecular chains, and the molecular chain structure remains relatively stable. However, the chain segments containing disulfide bonds have responded to the temperature change, and the thermal motion has begun to increase. The synergistic interaction with hydrogen bonds has led to the gradual expansion of the molecular chain space, and the degree of freedom of the molecular chain movement has been increased, which results in the gradual decrease of the energy storage modulus. In this process, the energy dissipation is mainly reflected in the small vibration and local friction of the chain segments. With the intensification of the effect of temperature on the hydrogen bonds, the damping effect of the synergistic movement of the chain segments is weakened, and the loss modulus also decreases slowly. Meanwhile, the hydrogen-bonding network formed by DPH still retains a certain degree of integrity and plays a part in the maintenance of the intermolecular chain connection. As the temperature rises further, the stabilizing effect of hydrogen bonds continues to decay, and the mobility of the rigid PAA structure in the PU chain begins to increase, so that the molecular chain segments can carry out the movement and rearrangement more freely, and the range of movement can be further expanded. The dynamic properties of the disulfide bonded chain segments are more and more prominent, and their fracture and reorganization processes are deeply involved in the arrangement of the molecular chains, which makes the decrease of the energy storage moduli more significant and gentler. From the perspective of energy dissipation, the changes in chain segment friction patterns and degrees, along with the continuous influence of the disulfide-bonding dynamic process, result in a gradual decrease in energy dissipation efficiency, and the loss modulus decreases steadily. Meanwhile, the dissociation degree of the hydrogen-bonding network formed by DPH continues to increase.

Overall, within the test range from −80 to 100 °C, the energy storage moduli of the PU elastomers are consistently

https://doi.org/10.1021/acs.macromol.5c00013
Macromolecules 2025, 58, 1425−1434

higher than the loss modulus. This indicates that they maintain a certain degree of mechanical strength and remain in a solid state throughout the entire test temperature range. Such a characteristic is conducive to enhancing the mechanical properties of the materials at room temperature without affecting their self-healing properties after being warmed up. Moreover, the mechanical properties of the elastomers can be regulated by adjusting the DPH content, which lays a solid foundation for the application of elastomers. As can be seen from Figure 3f, the elastomer has a glass transition temperature around −51 °C, which is lower than room temperature. Consequently, the PU is in the rubbery state at room temperature, and this is consistent with the results of the tensile curve exhibited by PU elastomers. Meanwhile, the relatively low T_g imparts good kinematics to the polymer chain segments, thereby enhancing the self-healing and recyclable properties of the material.

The mechanical properties of PU elastomers are influenced by triple interactions, namely, multiple hydrogen bonds, dynamic disulfide bonds, and rigid chain segments. The impacts of these factors on the mechanical properties of elastomers were explored by adjusting the contents of DPH and PAA. The stress−strain curves of all of the samples are presented in Figure 4a. None of the samples exhibited a yielding phenomenon, signifying that the synthesized PU is a typical elastomeric material. As illustrated in Figure 4b, the maximum tensile strength of the PU-3 sample reached 50.1 MPa, with an elongation at break of 830.7% and a toughness value of 144.2 MJ/m^3, which is considerably higher than those of many reported synthetic materials. The tensile strengths of PU-4 and PU-5 were 41.2 and 32.3 MPa, respectively. In comparison with PU-1, the tensile strengths of PU-4 and PU-5 were noticeably enhanced, while the elongation at break was remarkably decreased. The toughness increased due to the combined effect of the rigid chain segments and multiple acylcarbamoyl urea groups. It can be concluded that the tensile strength of PU elastomers rises with the increment of PAA chain segment content, whereas the elongation at break declines as the content of PAA goes up. During the copolymerization process of amino-terminated PAA oligomers serving as elastomer rigid segments, an addition reaction occurs between amino-terminated PAA and isocyanate-terminated PU prepolymers. The rigid chain segments construct a reinforcing framework, and simultaneously, the urethane bonds are formed to create a linear elastomer network, which gives rise to a stronger intermolecular chain interaction force. Since the rigid oligomer molecular chains are less mobile, the elongation at break decreases while the tensile strength increases. PAA possesses a more rigid structure than urea and urethane groups. Moreover, the carboxyl groups on PAA form hydrogen-bonding interaction with urea and urethane groups in the PU chain, leading to superior mechanical properties.

To demonstrate that the rigid PAA in the design strategy can enhance the mechanical properties of the materials, comparative samples without a DPH chain extender were synthesized, named PU-control-1 and PU-control-2, respectively. The corresponding stress−strain curves are shown in Figure S9. Both PU-control-2 and PU-control-1 exhibit typical tensile curves of elastomers, with breaking strengths of 26 and 12 MPa and elongations at break of 901% and 970%, respectively. The FTIR spectra (Figure S5, Supporting Imformation) of PU-control-1 and PU-control-2 exhibit peaks at 2260 cm^{-1}, which suggests the presence of unreacted isocyanate. In contrast, PU-2 shows neither such peaks nor any residual isocyanate, and it exhibits the highest tensile strength. Hence, it is demonstrated to be feasible to add PAA by mass to react with the prepolymer. The breaking strength of PU-2 is much higher than that of the comparison samples, and the mechanical strength gradually increases with the increase of the rigid PAA content, which proves the reasonableness of the strategy of the enhanced mechanical properties of rigid chain segments.

The self-healing ability of PU elastomers was measured by tensile tests at different self-healing times. To quantitatively assess the self-healing ability of elastomers, sample PU-3 with the highest tensile strength was selected for uniaxial tensile testing after different self-healing times. The stress−strain curves as in Figure 4c demonstrate the self-healing performance of PU-3 at 80 °C for different self-healing times, and the self-healing efficiency of the material gradually increases with the increase of time. As shown in Figure 4d, the best self-healing efficiency of PU-3 at 12 h is 96.1%. This is due to the strong internal hydrogen-bonding interactions and structural compactness. The self-healing mechanism of the material is attributed to the fact that when the damaged material is heated from room temperature to self-healing temperature, the hydrogen-bonding interactions between the polymer molecules are opened and the motility of the polymer chain segments is significantly stimulated, while the dynamic disulfide bonds undergo reorganization. As a result, the polymer chain segments at the wound can intersperse and diffuse, and the polymer structure at the wound is reconfigured as the self-healing time increases. When the elastomer is brought down to room temperature, the intermolecular interaction forces between the polymer chain segments are reformed, thus completing the self-healing process of the material. In addition, the PU elastomer in this work exhibits excellent mechanical properties and self-healing efficiency compared to the related literature reported, as shown in Figure 4e.

The samples were subjected to pairs of consecutive constant deformation load−unload tests and incremental load−unload cyclic tensile tests to assess their energy dissipation capabilities. Five consecutive 500% strain tensile cyclic tests were first performed as in Figure 4f. The elastomer exhibited a large hysteresis loop during the first cycle, which indicated a large energy dissipation due to the breaking of noncovalent interactions within the polymer chains. The hysteresis loop gradually decreases with the number of cycles, as the noncovalent interactions cannot be quickly and fully restored to their original state. Although a large cyclic hysteresis is exhibited between the first and second cycles, the hysteresis is significantly smaller at the initial point of the second cycle. In addition, the start and end points of the last three cycles of PU-3 are more concentrated than those of the previous cycle, and the overlap of the last three cycles is better, which implies that PU-3 has a better recovery from deformation and a greater energy dissipation. More specifically, the aggregated state of PU-3 reduces chain segment slippage and improves elastic properties. The elastomer at this ratio achieves unity of the mechanical properties and elasticity. Next, loading and unloading cyclic tests were performed with strain increasing from 100% to 800% without delay time. Figure 4g shows that the hysteresis loop increases gradually with increasing strain with less dissipation at low strains and more dissipation at high strains. The loosely cross-linked chemical network acts as a

https://doi.org/10.1021/acs.macromol.5c00013
Macromolecules 2025, 58, 1425−1434

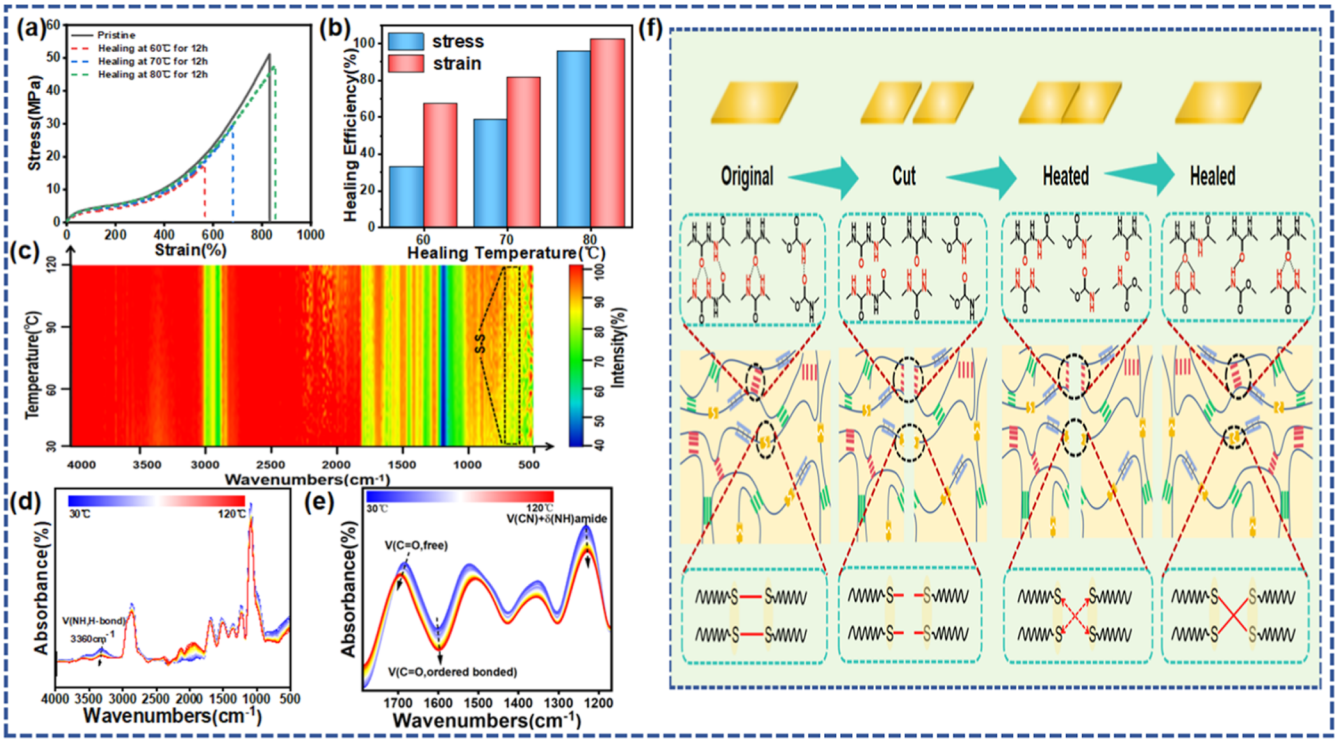

Figure 5. Self-healing properties. (a) Self-healing stress−strain curves; (b) self-healing efficiency bar chart; (c) two-dimensional variable-temperature infrared image; (d) variable-temperature infrared spectrum of PU-3 in the range of 30 to 120 °C; (e) variation of temperature-dependent FTIR spectra of PU-3 in the range of 1780−1170 cm^{-1} heating from 30 to 120 °C; (f) proposed self-healing mechanism of PU-3.

strong molecular framework to resist deformation and maintain the elasticity of the self-healing polymer. At the same time, the high density of hydrogen bonds formed by the sextuple hydrogen-bonding units in the PU chains contributes to the excellent toughness. During stretching, hydrogen bonds not only reconstitute quickly after fracture but also act as weak dynamic bonds to dissipate strain energy and increase toughness, thus maintaining the basic structure of the hard segments and endowing the material with excellent self-healing capabilities and high stress properties.

To assess the dynamic loading behavior of the elastomers, crack extension experiments were carried out on PU-3. Subsequently, fracture energy measurements were conducted to quantitatively assess the crack resistance. The elastomers exhibited excellent tear resistance, mainly because their excellent energy dissipation capability enabled them to absorb and disperse the energy generated during the tearing process effectively. As shown in Figure 4h, the elastomer sample with a 1 mm notch can be stretched to 9.1 times its original length. Calculations based on stress−strain curves before and after fracture were conducted. The results show that the elastomer has a maximum fracture energy of 77.18 $kJ·m^2$. This indicates excellent fracture toughness and notch insensitivity, as shown in Figure 4i. The dynamic rigid segment in the polymer network achieved crack bridging through the entangled sliding of the molecular chains. Moreover, as the elongation increased, the fracture stress concentrated at the crack tip was effectively transferred to the entire elastomer network. This deflected the cracking from the original tearing direction and retarded the transverse extensional motion of the crack tip, thereby improving the mechanical properties of the notched material. These results indicate that the fracture energy is caused by the unique internal structure of the rigid segments and that the designed network polymer elastomers have excellent flexibility and tear resistance.

Due to the sextuple hydrogen-bonding unit and disulfide bond unit of DPH, PU displays excellent self-healing properties. Variable-temperature infrared thermography was employed to investigate the self-healing behavior of incisions on elastomer films, with the aim to explore the self-healing mechanism. PU-3 elastomers with remarkable mechanical properties exhibited a good self-healing ability. The cuts of completely fractured elastomers were rejoined and placed on a heated stage for a certain period of time to evaluate this ability. By observing the self-healing process of PU-3 at different temperatures such as 60 °C, 70 °C, and 80 °C for 12 h, respectively, it was discovered that the tensile strength and elongation at break presented a gradually increasing tendency with the elevation of the self-healing temperature. As depicted in Figure 5a, the stress−strain curve of PU-3 was obtained after 12 h of self-healing at 80 °C. And as shown in Figure 5b, the highest self-healing efficiency of 96.1% was attained at 80 °C. Appropriately increasing the heating temperature is beneficial for enhancing the self-healing rate of PU-3, as it can promote the reversible breakage of hydrogen and disulfide bonds, accelerating the chain segment movement and chain rearrangement. In the two-dimensional infrared image of Figure 5c, a significant intensity variation of the infrared absorption peak of S−S bonds can be observed around 640 cm^{-1} during the temperature increase from 30 to 120 °C. The intensity change becomes more prominent with the temperature rise, suggesting that S−S bonds persist throughout the temperature change and that the chain exchange reaction of breaking and reorganizing to form new S−S bonds is continuously carried out. During the heating process, the cracks at the fracture of the samples achieved complete self-healing. Furthermore, the self-healing

https://doi.org/10.1021/acs.macromol.5c00013
Macromolecules 2025, 58, 1425−1434

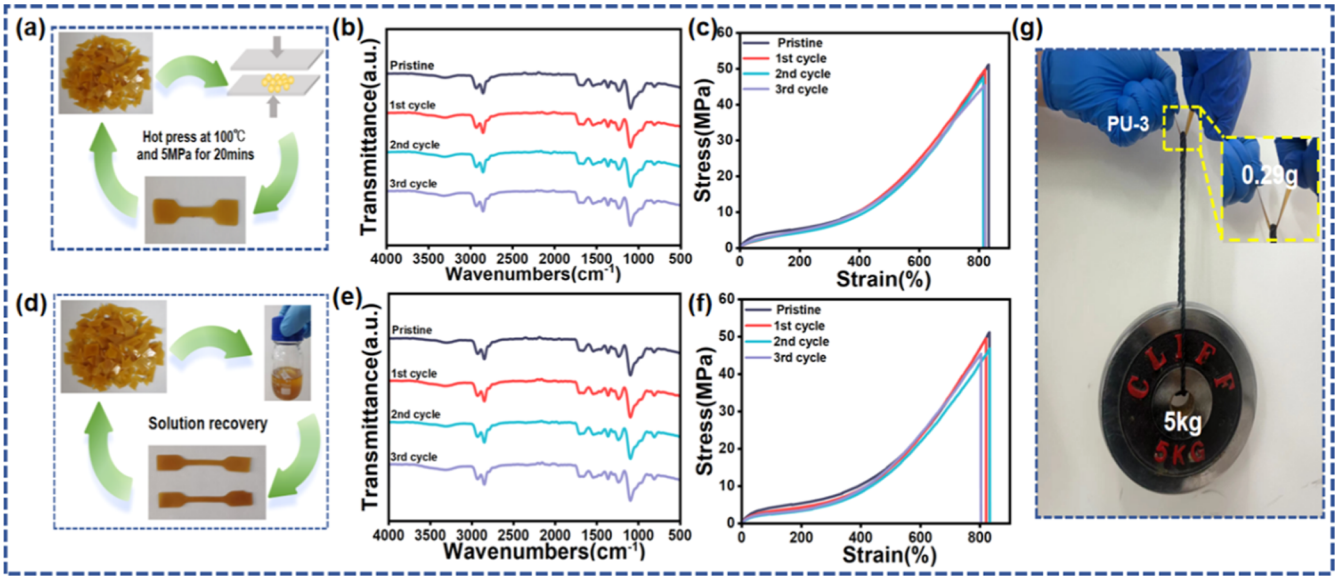

Figure 6. Recyclable properties. (a) Hot-pressing recovery diagram; (b) hot-pressing cycle stretching image; (c) hot-pressing cycle infrared image; (d) solution recovery diagram; (e) solution recovery cycle stretching image; (f) solution recovery cycle infrared image; (g) digital photograph demonstrating that the PU-3 sheet lifts a weight of 5 kg without fracture.

mechanism can also be elucidated by variable-temperature infrared stacking thermograms. As illustrated in Figure 5d, with the increase of the temperature from 30 to 120 °C, the absorption peak at 3360 cm^{-1} corresponding to the N−H stretching vibration gradually diminishes with the temperature increase and the breakage of self-reinforcing complementary hydrogen bonds in the polymer, mainly due to the stretching vibration and bending vibration of the N−H group. Meanwhile, it can be seen in Figure 5e that only the intensity of the absorption band of the free C═O group (1708 cm^{-1}) gradually augments and undergoes a significant blue shift, whereas the intensity of the absorption peaks of the hydrogen-bonded C═O groups (1636 and 1622 cm^{-1}) shows a remarkable decrease but no shift. These results imply that when the temperature is increased, the hydrogen-bonding interactions at the damage site of elastomers can be disrupted. This endows the polymer chain segments with a high diffusion ability. Then, the movement of the polymer chain segments at the damaged site enables them to intermingle and intertwine. Subsequently, the hydrogen-bonding interactions can be re-established at the damage site of the elastomer, ultimately achieving the self-healing behavior. Therefore, the primary reason for the excellent mechanical strength and high self-healing efficiency is that the high density of hydrogen bonds in the hard segments exhibits dynamic characteristics that permit the reversible fracture and reorganization of heat-activated hydrogen bonds. The results demonstrate that the self-healing capability of PU mainly stems from the synergistic effect of multiple hydrogen bonds and dynamic disulfide bonds.

The specific principle and process of the PU-3 chain containing S−S bond exchange reaction are illustrated in Figure 5f. During the heating process, the S−S bonds break, giving rise to two broken bonds. When the cross sections are joined together, the broken S−S bonds overlap and recombine under the stimulation of continuous heating, thereby forming new S−S bonds. Meanwhile, the hydrogen-bonding interactions at the fracture sites open and reorganize. As a result, PU-3 undergoes a dynamic self-healing process from the inside out. This provides a valuable research basis for the field of chemically modified self-healing materials with rigid chain segments.

The dynamic properties possessed by multiple hydrogen bonds and disulfide bonds in PU-3 elastomers synergize with each other effectively to create conditions for the recycling of the material. This synergy then enables the recycling of PU-3 elastomers by both solution and hot-pressing processes. In the recycling performance study, FTIR spectral analysis and a stress−strain curve test were executed on the recycled elastomers. As shown in Figure 6a, hot pressing of the fragments at 100 °C and 5 MPa pressure for 30 min reconverted the fragments into intact PU-3 films. As shown in Figure 6b, the locations and intensities of the main characteristic peaks of the FTIR of the PU-3 elastomer after hot-press recycling were almost the same as those of the pristine elastomer. Meanwhile, stress−strain tests were performed on the hot-pressing elastomers. As shown in Figure 6c, the stress−strain curves were comparable to those of the pristine materials in terms of tensile strength and elongation at break variations. Even after the three shredding recycling cycles, the performance remained comparable to that of the original samples. In addition, the elastomer can be recovered by the solvent-assisted method as shown in Figure 6d. The PU-3 elastomer fragments were dissolved in DMAc at 80 °C and stirred well. Then, the solution was slowly cast onto a clean and dry glass substrate and dried to reclaim the intact elastomer film. After three recoveries, the films were analyzed by FTIR, as shown in Figure 6e, which indicated that the positions and relative intensities of the characteristic absorption peaks of each major functional group were consistent with those of the original samples. As shown in the stress−strain curve of Figure 6f, the tensile strength and elongation at break of the elastomer were comparable with those of the original material. Moreover, as shown in Figure 6g, the solution-recovered PU elastomer PU-3 can easily hang 5 kg dumbbells without breaking. All of the above results show the good recyclability of PU-3, which meets the demand for high-performance recyclable materials in different industrial fields.

https://doi.org/10.1021/acs.macromol.5c00013
Macromolecules 2025, 58, 1425−1434

4. CONCLUSIONS

In this study, the PU elastomer with high-strength and self-healing properties is successfully prepared by gradual copolymerization of rigid PAA and flexible PU chain segments, which provides a new strategy for the preparation of PU with high-strength, high self-healing efficiency, and recycling properties. Its tensile strength reaches 50.1 MPa, toughness is 144.2 MJ/m^3, elongation at break is about 830%, and fracture energy reaches 77.18 $kJ·m^2$. Moreover, the self-healing efficiency is as high as 96.1% after 12 h of healing at 80 °C. The rigid chain segments of PAA, serving as the backbone, not only give the material excellent tear resistance, good ductility, and toughness but also enable energy to be dissipated through structural deformation and chain stretching when the material is subjected to stress. The elastomer has the characteristics of heating to heal mechanical damage and efficient recycling ability, and it was able to maintain the efficient mechanical properties after three cycles of solvent recovery and hot press recovery. The design strategy of the rigid chain segment structure and noncovalent cross-linking synergistically strengthening the strength of flexible polymers provides a universal idea for the development of other high-strength elastomers, which is expected to promote the innovative development and technological progress in the field of PU elastomers, reduce the consumption of raw materials, and prolong the service life of materials.

■ ASSOCIATED CONTENT

Data Availability Statement

All data needed to evaluate the conclusions in the paper are present in the paper and/or the Supporting Information.

Supporting Information

The Supporting Information is available free of charge at https://pubs.acs.org/doi/10.1021/acs.macromol.5c00013.

Additional detailed experimental data including synthesis procedures, synthesis formula, and characterization; ^{1}H NMR spectra of monomers; GPC results of the monomers; FTIR spectra of PU polymer; TGA curves and DTG curves of PU polymer; and stress−strain curves of PU polymer (PDF)

■ AUTHOR INFORMATION

Corresponding Author

Hui Zhao − *School of Light Industry and Food Engineering, Guangxi University, Nanning 530004, China;* orcid.org/0000-0001-8554-9411; Email: zhh@gxu.edu.cn

Authors

Li-Quan Huang − *School of Light Industry and Food Engineering, Guangxi University, Nanning 530004, China*

Hua-Xin Huang − *School of Light Industry and Food Engineering, Guangxi University, Nanning 530004, China*

Ning Yu − *School of Light Industry and Food Engineering, Guangxi University, Nanning 530004, China*

Chang-Zhou Chen − *School of Light Industry and Food Engineering, Guangxi University, Nanning 530004, China;* orcid.org/0000-0001-7675-4368

Yang Liu − *School of Light Industry and Food Engineering, Guangxi University, Nanning 530004, China;* orcid.org/0000-0001-8104-6462

Guo-Hua Hu − *Laboratory of Reactions and Process Engineering, CNRS-University of Lorraine, Nancy 54001, France;* orcid.org/0000-0002-1001-6386

Jun Du − *Guangxi Key Laboratory of Advanced Structural Materials and Carbon Neutralization, School of Materials and Environment, Guangxi Colleges and Universities Key Laboratory of Environmental-friendly Materials and New Technology for Carbon Neutralization, Guangxi Minzu University, Nanning 530105, China*

Complete contact information is available at: https://pubs.acs.org/10.1021/acs.macromol.5c00013

Author Contributions

‖L.-Q.H. and H.-X.H. contributed equally to this work. **Li-Quan Huang**: Data curation, formal analysis, writing—original draft, and writing—review and editing. **Hua-Xin Huang**: Investigation, writing—original draft, and writing—review and editing. **Ning Yu**: Data curation and formal analysis. **Chang-Zhou Chen**: Resources and software. **Yang Liu**: Investigation and methodology. **Jun Du**: Supervision, validation, and visualization. **Guo-Hua Hu**: Methodology and project administration. **Hui Zhao**: Validation, visualization, and project administration.

Notes

The authors declare no competing financial interest.

■ ACKNOWLEDGMENTS

This work was supported by the National Natural Science Foundation of China (No. 22268009), Guangxi Natural Science Foundation Program (Nos 2024GXNSFAA010367, 2024JJG160026, and 2024AB33198), and Opening Project of Guangxi Key Laboratory of Calcium Carbonate Resources Comprehensive Utilization (No. HZXYKFKT202204).

■ REFERENCES

(1) Hu, S.; He, S.; Wang, Y.; Wu, Y.; Shou, T.; Yin, D.; Mu, G.; Zhao, X.; Gao, Y.; Liu, J.; et al. Self-repairable, recyclable and heat-resistant polyurethane for high-performance automobile tires. *Nano Energy* **2022**, *95*, 107012.

(2) Herzberger, J.; Sirrine, J. M.; Williams, C. B.; Long, T. E. Polymer design for 3D printing elastomers: Recent advances in structure, properties, and printing. *Prog. Polym. Sci.* **2019**, *97*, 101144.

(3) Olaleye, K.; Junik, K.; Duda, S.; Jamroziak, K.; Lesiuk, G. Experimental and numerical investigation on fatigue behavior of pur (rigid polyurethane) elastomers 90sha used in automotive engineering. *Alexandria Eng. J.* **2024**, *109*, 963−969.

(4) Xu, L.; Shao, S.; Lu, X.; Wang, D.; Zhang, A.; Zhang, J. Wrinkle-enabled hydrophobic underwater stable ionic skin with unique positive resistance effect. *Chem. Eng. J.* **2024**, *496*, 153454.

(5) Zhu, Y.; He, Y.; Lu, W.; Tian, H.; Fei, F.; Zhou, P.; Wang, J. Multi-functional self-healing polyurethane elastomer based on chair conformation for strain sensors. *J. Mater. Chem. A* **2024**, *12* (42), 28716−28730.

(6) Li, H.; Le, J.; Tan, H.; Hu, L.; Li, X.; Zhang, K.; Zeng, S.; Liu, Q.; Zhang, M.; Shi, L.; et al. Synergistic multimodal energy dissipation enhances certified efficiency of flexible organic photovoltaics beyond 19%. *Adv. Mater.* **2024**, 2411989.

(7) Chu, C.; Sun, W.; Chen, S.; Jia, Y.; Ni, Y.; Wang, S.; Han, Y.; Zuo, H.; Chen, H.; You, Z.; et al. Squid-inspired anti-salt skin-like elastomers with superhigh damage resistance for aquatic soft robots. *Adv. Mater.* **2024**, *36* (44), 2406480.

(8) Guo, Y.; Yang, L.; Zhang, L.; Chen, S.; Sun, L.; Gu, S.; You, Z. A dynamically hybrid crosslinked elastomer for room-temperature recyclable flexible electronic devices. *Adv. Funct. Mater.* **2021**, *31* (50), 2106281.

(9) Li, C.; Yang, X.; Wang, Y.; Liu, J.; Zhang, X. Core−shell nanostructured assemblies enable ultrarobust, notch-resistant and self-healing materials. *Adv. Mater.* **2024**, *34* (52), 2410659.
(10) Chen, S.; Wang, Y.; Yang, L.; Chu, C.; Cao, S.; Wang, Z.; Xue, J.; You, Z. Biodegradable elastomers for biomedical applications. *Prog. Polym. Sci.* **2023**, *147*, 101763.
(11) Ye, H.; Zhang, K.; Kai, D.; Li, Z.; Loh, X. J. Polyester elastomers for soft tissue engineering. *Chem. Soc. Rev.* **2018**, *47* (12), 4545−4580.
(12) Liu, K.; Wang, M.; Huang, C.; Yuan, Y.; Ning, Y.; Zhang, L.; Wan, P. Flexible bioinspired healable antibacterial electronics for intelligent human-machine interaction sensing. *Adv. Sci.* **2023**, *11* (10), 2305672.
(13) Guo, X.; Liang, J.; Wang, Z.; Qin, J.; Zhang, Q.; Zhu, S.; Zhang, K.; Zhu, H. Tough, recyclable, and degradable elastomers for potential biomedical applications. *Adv. Mater.* **2023**, *35* (20), 2210092.
(14) Wang, X.; Zhan, S.; Lu, Z.; Li, J.; Yang, X.; Qiao, Y.; Men, Y.; Sun, J. Healable, recyclable, and mechanically tough polyurethane elastomers with exceptional damage tolerance. *Adv. Mater.* **2020**, *32* (50), 2005759.
(15) Wang, X.; Sun, J. Engineering of reversibly cross-linked elastomers toward flexible and recyclable elastomer/carbon fiber composites with extraordinary tearing resistance. *Adv. Mater.* **2024**, *36* (35), 2406252.
(16) Wang, X.; Xu, J.; Zhang, Y.; Wang, T.; Wang, Q.; Li, S.; Yang, Z.; Zhang, X. A stretchable, mechanically robust polymer exhibiting shape-memory-assisted self-healing and clustering-triggered emission. *Nat. Commun.* **2023**, *14* (1), 4712.
(17) Zhang, M.; Wang, Y.; Yang, M.; Sun, L.; Zhao, G.; Feng, P.; Li, N.; Liu, C.; Xu, J.; Jian, X.; et al. Construction of mechanical robust elastomers by simulating the strengthening and healing process of natural skin toward multifunctional electronics. *Macromolecules* **2024**, *57* (7), 3047−3057.
(18) Zhu, X.; Han, K.; Li, C.; Wang, J.; Yuan, J.; Pan, Z.; Pan, M. Tough, photoluminescent, self-healing waterborne polyurethane elastomers resulting from synergistic action of multiple dynamic bonds. *ACS Appl. Mater. Interfaces* **2023**, *15* (15), 19414−19426.
(19) Lv, D.; Li, X.; Huang, X.; Cao, C.; Ai, L.; Wang, X.; Ravi, S. K.; Yao, X. Microphase-separated elastic and ultrastretchable ionogel for reliable ionic skin with multimodal sensation. *Adv. Mater.* **2023**, *36* (17), 2309821.
(20) Wu, H.; Wang, H.; Luo, M.; Yuan, Z.; Chen, Y.; Jin, B.; Wu, W.; Ye, B.; Zhang, H.; Wu, J. Mechanically robust, self-reporting and healable polyurethane elastomers by incorporating symmetric/asymmetric chain extenders. *Mater. Horiz.* **2024**, *11* (6), 1548−1559.
(21) Qin, J.; Chen, Y.; Guo, X.; Huang, Y.; Chen, G.; Zhang, Q.; He, G.; Zhu, S.; Ruan, X.; Zhu, H. Regulation of hard segment cluster structures for high-performance poly(urethane-urea) elastomers. *Adv. Sci.* **2024**, *11* (22), 2400255.
(22) Yang, W.; Lu, B.; Zhu, Y.; Yang, Y.; Puglia, D.; Xa, P.; Liu, T.; Ma, P. A fully healable, mechanical self-strengthening and antibacterial poly(thiocarbamate-urethane) elastomer constructed via dual reversible dynamic networks. *Chem. Eng. J.* **2024**, *482*, 149179.
(23) Chen, J.; Li, C.; Jia, H.; Shen, Z.; Zhao, R.; Su, T.; Xiang, B.; Wang, X.; Boukhvalov, D. W.; Luo, Z.; et al. Novel molecular-level insight into the self-healing behavior and mechanism of polyurethane-urea elastomer based on a noncovalent strategy. *Macromolecules* **2022**, *55* (11), 4776−4789.
(24) Xu, X.; Zhao, H.; Ji, S.; Li, S.; Zhang, L.; Wen, S.; Liu, J. High-strength, self-healing waterborne polyurethane elastomers with enhanced mechanical, thermal, and electrical properties. *Compos. Commun.* **2024**, *51*, 102100.
(25) Yang, Y.; Li, X.; Jiang, H.; Ge, M.; Su, X.; Zou, M.; Li, G. Carbon nanotubes grafted by polyurethane chains with dopamine-mediation to enhance the mechanical and damping properties of polyurethane elastomer. *Polymer* **2023**, *280*, 126041.
(26) Meganathan, M. K.; Sasikala, H.; Ramalingam, S. Self-healable UV-triggered silica−polyurethane nanocomposite-reinforced fabric coating: Implications for protective fabrics. *ACS Appl. Nano Mater.* **2024**, *7* (24), 28713−28724.
(27) Bai, J.; Gu, W.; Bai, Y.; Li, Y.; Yang, L.; Fu, L.; Li, S.; Li, T.; Zhang, T. Multifunctional flexible sensor based on PU-ta@MXene janus architecture for selective direction recognition. *Adv. Mater.* **2023**, *35* (35), 2302847.
(28) Das, P.; Marvi, P. K.; Ganguly, S.; Tang, X.; Wang, B.; Srinivasan, S.; Rajabzadeh, A. R.; Rosenkranz, A. MXene-based elastomer mimetic stretchable sensors: Design, properties, and applications. *Nano-Micro Lett.* **2024**, *16* (1), 135.
(29) Li, N.; Yuan, X.; Li, Y.; Zhang, G.; Yang, Q.; Zhou, Y.; Guo, M.; Liu, J. Bioinspired Liquid Metal Based Soft Humanoid Robots. *Adv. Mater.* **2024**, *36* (35), 2407170.
(30) Li, X.; Wang, Y.; Zhang, X. Strong, healable materials with bio-like ordered architectures and versatile functionality. *SusMat* **2024**, *4* (6), No. e248.
(31) Wang, H.; Huang, J.; Liu, W.; Huang, J.; Yang, D.; Qiu, X.; Zhang, J. Tough and fast light-controlled healable lignin-containing polyurethane elastomers. *Macromolecules* **2022**, *55* (19), 8629−8641.
(32) Song, P.; Wang, H. High-performance polymeric materials through hydrogen-bond cross-linking. *Adv. Mater.* **2019**, *32* (18), 1901244.
(33) Yao, Y.; Liu, B.; Xu, Z.; Yang, J.; Liu, W. An unparalleled h-bonding and ion-bonding crosslinked waterborne polyurethane with super toughness and unprecedented fracture energy. *Mater. Horiz.* **2021**, *8* (10), 2742−2749.
(34) Wang, L.; Guo, L.; Zhang, K.; Xia, Y.; Hao, J.; Wang, X. Development of tough thermoplastic elastomers by leveraging rigid−flexible supramolecular segment interplays. *Angew. Chem., Int. Ed.* **2023**, *62* (29), No. e202301762.
(35) Ou, F.; Xie, T.; Li, X.; Zhang, Z.; Ning, C.; Tuo, L.; Pan, W.; Wang, C.; Duan, X.; Liang, Q.; et al. Liquid-free ionic conductive elastomers with high mechanical properties and ionic conductivity for multifunctional sensors and triboelectric nanogenerators. *Mater. Horiz.* **2024**, *11* (9), 2191−2205.
(36) Song, L.; Zhu, T.; Yuan, L.; Zhou, J.; Zhang, Y.; Wang, Z.; Tang, C. Ultra-strong long-chain polyamide elastomers with programmable supramolecular interactions and oriented crystalline microstructures. *Nat. Commun.* **2019**, *10* (1), 1315.
(37) Zhou, K.; Zhang, Q.; Gong, J.; Shen, H.; Luo, H.; Chen, S.; Zhang, X.; Zhang, N.; Pei, X.; Wang, T.; et al. Dynamic non-covalent bonds powering enhanced temporary shape retention temperature and mechanical robustness in shape memory polyurethane. *ACS Appl. Mater. Interfaces* **2024**, *16* (46), 64031−64041.
(38) Li, F.; Wang, L.; Gao, L.; Zu, D.; Zhang, D.; Xu, T.; Hu, Q.; Zhu, R.; Liu, Y.; Hu, B. L. Reducing dielectric loss of high-dielectric-constant elastomer via rigid short-chain crosslinking. *Adv. Mater.* **2024**, *36* (47), 2411082.
(39) Li, H.-W.; Zhang, J.-L.; Xue, R.; An, Z.-W.; Wu, W.; Liu, Y.; Hu, G.-H.; Zhao, H. Construction of self-healable and recyclable waterborne polyurethane-MOF membrane for adsorption of dye wastewater based on solvent etching deposition method. *Sep. Purif. Technol.* **2023**, *320*, 124145.
(40) Wang, C.; Duan, X.; Li, X.; Pan, W.; Ning, C.; Wang, F.; Cao, W.; Ou, F.; Wang, M.; Liang, Q.; et al. A self-healing solid-state ion-conductive elastomer with high mechanical robustness and high conductivity for soft ionotronics. *Adv. Funct. Mater.* **2024**, *34* (38), 2402815.
(41) Zhao, H.; Li, K.-C.; Wu, W.; Li, Q.; Jiang, Y.; Cheng, B.-X.; Huang, C.-X.; Li, H.-N. Microstructure and viscoelastic behavior of waterborne polyurethane/cellulose nanofiber nanocomposite. *J. Ind. Eng. Chem.* **2022**, *110*, 150−157.
(42) Cheng, B.-X.; Zhang, J.-L.; Jiang, Y.; Wang, S.; Zhao, H. High toughness, multi-dynamic self-healing polyurethane for outstanding energy harvesting and sensing. *ACS Appl. Mater. Interfaces* **2023**, *15* (50), 58806−58814.

https://doi.org/10.1021/acs.macromol.5c00013
Macromolecules 2025, 58, 1425−1434